Thermogravimetry study of Gd_2O_3 chlorination

Federico J. Pomiro, Gastón G. Fouga, Juan P. Gaviría & Ana E. Bohé

Journal of Thermal Analysis and Calorimetry
An International Forum for Thermal Studies

ISSN 1388-6150
Volume 122
Number 2

J Therm Anal Calorim (2015)
122:679-687
DOI 10.1007/s10973-015-4738-2

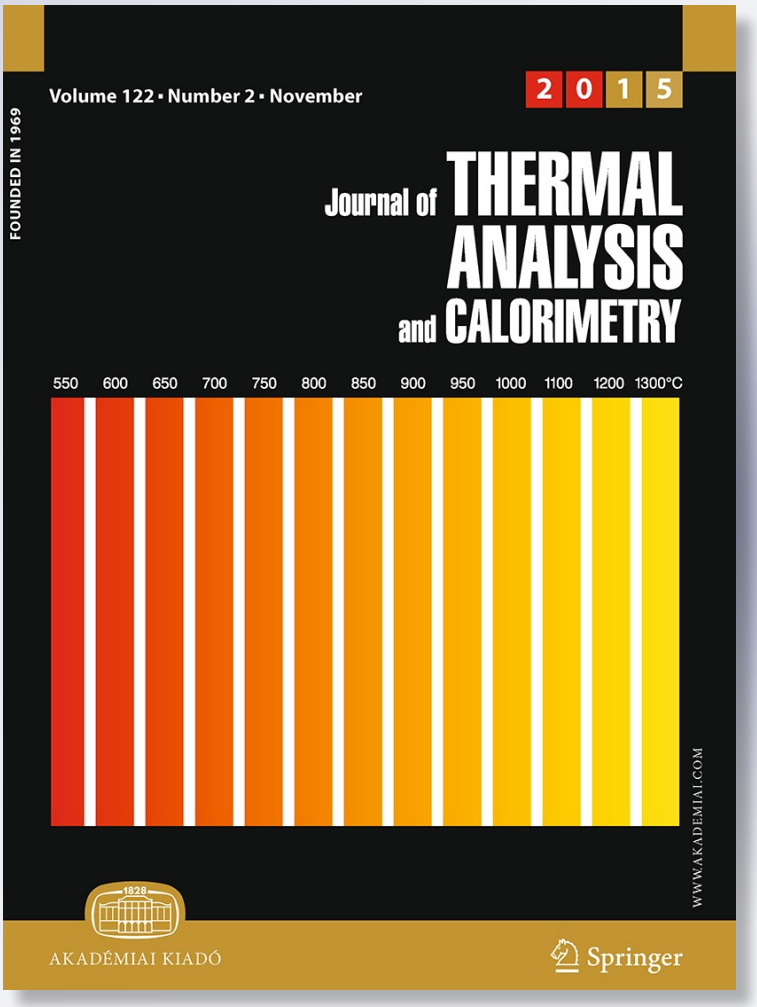

Springer

J Therm Anal Calorim (2015) 122:679–687
DOI 10.1007/s10973-015-4738-2

Thermogravimetry study of Gd_2O_3 chlorination

Kinetics and characterization of gadolinium oxychloride

Federico J. Pomiro[1] · Gastón G. Fouga[1,2] · Juan P. Gaviría[1,2] · Ana E. Bohé[1,2,3]

Received: 27 November 2014 / Accepted: 1 May 2015 / Published online: 28 May 2015

Abstract The reaction between Gd_2O_3(s) and Cl_2(g) was studied in a high-resolution thermogravimetric system. The reaction product was GdOCl, which was the unique solid phase produced in all the temperature range studied. The GdOCl is subsequently chlorinated producing $GdCl_3$ for temperatures above 1123 K. The system is under chemical control for temperatures below 723 K. It was found that the reaction order with respect to the chorine partial pressure is 0.77 and the activation energy is 132 kJ mol^{-1} for the temperature range of 623–723 K. The global rate equation was developed. The GdOCl obtained was characterized by X-ray diffraction, scanning electron microscopy and magnetic measurements. The structure of GdOCl was refined with the Rietveld method, and it crystallized in a tetragonal form of REOX possessing the Matlockite-type (PbFCl) structure. The magnetic measurements indicated that the sample is paramagnetic at all the measurement ranges. The parameters of the Curie–Weiss law obtained were as follows: $\theta = -12.0$ K, $C = 7.9592$ emu K mol^{-1} and $\mu_{eff} = 7.98\mu_B$.

✉ Federico J. Pomiro
pomiro@cab.cnea.gov.ar

[1] Departamento de Fisicoquímica y Control de Calidad, Complejo Tecnológico Pilcaniyeu, Centro Atómico Bariloche, Comisión Nacional de Energía Atómica, Av. Bustillo 9500, 8400 San Carlos de Bariloche, Río Negro, Argentina

[2] Consejo Nacional de Investigaciones Científicas y Técnicas (CONICET), Buenos Aires, Argentina

[3] Centro Regional Universitario Bariloche, Universidad Nacional del Comahue, 8400 San Carlos de Bariloche, Río Negro, Argentina

Keywords Gadolinium · Oxychloride · Chlorination · Kinetics · Chlorine · Rare earths

Introduction

Due to the electronic, magnetic, luminescent and catalytic properties of oxides, halides and oxyhalides of lanthanides, its consumption volume is increased in the last years [1–3]. Among rare earths (REs), gadolinium was found to play an important role in manufacturing appliances, computer hardware, metalworking, photoenergy production and medical imaging [4, 5].

Mutual separation of RE elements would be one of the most difficult problems in inorganic separation and extraction. Feasible alternative that allows the selective extraction of these metals from the respective ores and concentrates, as well as the refining and recovering of them from slags, is the application of chlorination and carbochlorination processes. Both processes are well-known dry methods for producing metal chlorides. The advantages of the chlorination technology are related to low-temperature operation, flexibility to raw material composition and selectivity of the process [1, 6–10].

TG methods, such as isothermal and non-isothermal methods, have been used widely to establish the kinetics for a conversion of many solids, including RE compounds [11–15]. The aim of the present paper is the kinetics study of the Gd_2O_3 chlorination in order to find the rate equation and subsequent characterization of GdOCl obtained.

The RE oxycompounds doped with trivalent RE ions are widely applied as commercial phosphors [16, 17]. The structural, magnetic and spectroscopic investigations of the product obtained of the Gd_2O_3 chlorination, gadolinium oxychloride, will permit its characterization and the

obtaining of structural crystallographic parameters, which are important for their possible uses.

Thermodynamic evaluation

A preliminary thermodynamic analysis of the potential reactions that could take place in the $Gd_2O_3(s)$–$Cl_2(g)$ system was made. The considered gadolinium oxide chlorination reactions were those which contemplate the formation of gadolinium chloride and oxychloride. The thermodynamic calculations were performed using the HSC Chemistry 6.1 software for windows [18].

The possible reactions in the $Gd_2O_3(s)$–$Cl_2(g)$ system are:

$$Gd_2O_3(s) + Cl_2(g) \rightarrow 2GdOCl(s) + 1/2O_2(g) \quad (1)$$

$$2/3Gd_2O_3(s) + Cl_2(g) \rightarrow 3/2GdCl_3(s,l) + O_2(g) \quad (2)$$

$$GdOCl(s) + Cl_2(g) \rightarrow GdCl_3(s,l) + 1/2O_2(g) \quad (3)$$

Figure 1 shows the Ellingham diagram for Eqs. 1–3. They summarize the evolution of standard free energy changes per mol of chlorine, ΔG^0, as a function of temperature. The curves show that the chlorination reactions that produces GdOCl(s) and $GdCl_3$(s,l) have negative ΔG^0 values, indicating that they are thermodynamically favorable; however, the formation of GdOCl(s) has the highest thermodynamic tendency to be produced in all temperature range studied.

Figure 2 shows the phase stability diagrams of Gd–Cl–O system at 723 and 1023 K. The axes of the diagrams are the partial pressure logarithm of O_2(g) and Cl_2(g). At the beginning of the chlorination reactions, the values of partial pressure of Cl_2(g) and O_2(g) were 0.35 and 10^{-4} atm, respectively, and these are indicated by an asterisk in the diagram (O_2(g) is

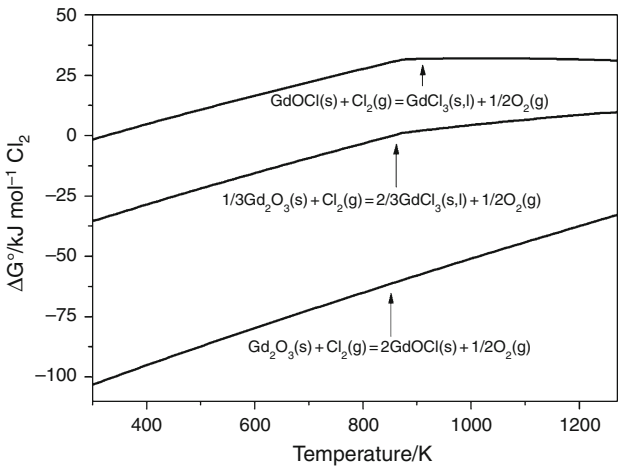

Fig. 1 Ellingham diagram for the reactions involved in the Gd_2O_3–$Cl_2(g)$ system

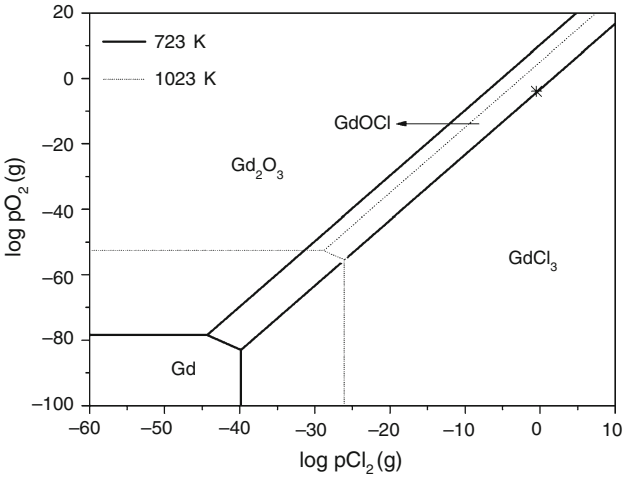

Fig. 2 Phase stability diagrams of Gd–Cl–O system at 723 and 1023 K

present in Ar(g) as an impurity). The possible stable condensed phases are Gd_2O_3(s), GdOCl(s) and $GdCl_3$(s,l). The phase stability diagrams show that there is not a thermodynamic equilibrium between Gd_2O_3(s) and $GdCl_3$(s,l). Therefore, GdOCl(s) has to be formed prior to the formation of $GdCl_3$(s,l) from the direct chlorination of Gd_2O_3(s).

Synthesis of gadolinium oxychloride and kinetics of the Gd_2O_3 chlorination

The gadolinium oxychloride, GdOCl, was prepared by the reaction of gadolinium oxide (99.9 % purity, SIGMA) in argon–chlorine atmosphere with different Cl_2(g) partial pressures. The Gd_2O_3 chlorination reactions were followed by a high-resolution thermogravimetric analyzer (TGA, model 2000, Cahn Instruments Inc.). This experimental setup has a sensitivity of ±5 μg under a gas flow rate between 2 and 8 L h^{-1} (measured under normal conditions of temperature and pressure) in the range of room temperature to 1223 K. Each sample was placed in a cylindrical silica glass crucible (diameter = 0.72 cm, high = 0.42 cm), which hangs from one of the arms of the electrobalance through a silica glass wire.

Non-isothermal reaction: onset temperature of chlorination reaction

Non-isothermal TG analyses were performed from room temperature to 1223 K. The experimental conditions were as follows: a linear heating rate of $\Delta T/\Delta t = 5.3$ K min^{-1}; Cl_2(g)–Ar(g) flow = 4 L h^{-1}, $m_0 = 10$ mg and $PCl_2 =$ 35 kPa. Figure 3 shows the percent relative mass change as a function of temperature. The reaction starts at approximately

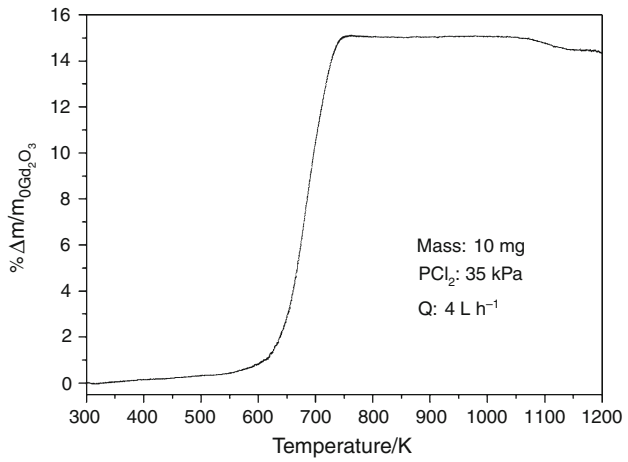

Fig. 3 TG curve for non-isothermal chlorination of Gd_2O_3

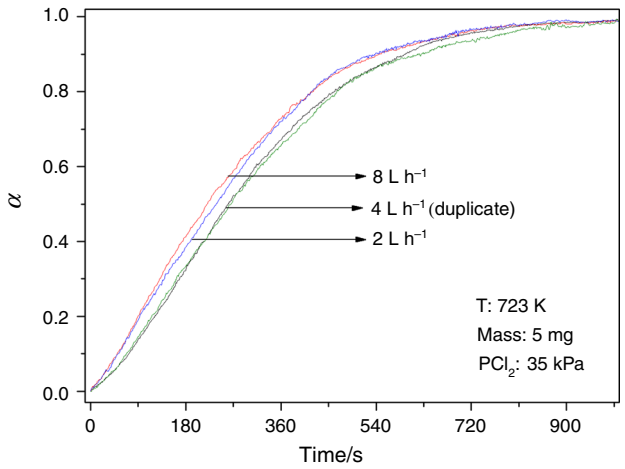

Fig. 4 Influence of gaseous flow rate in the chlorination of Gd_2O_3

600 K, showing a sharp mass increase until the relative mass change reaches a maximum value of $\%\Delta m/m_{0Gd_2O_3} = 15.1$. This value coincided with the stoichiometry mass change due to reaction 1.

The chlorination product was GdOCl, and it will be characterized in the following sections.

Also, in the non-isothermal curve is observed a decrease in the relative mass for temperatures above 1073 K. This phenomenon will be explained in section concerning this temperature range.

The reaction degree is given by $\Delta m_{Gd_2O_3}/m_{0Gd_2O_3}$, where $\Delta m_{Gd_2O_3}$ is the Gd_2O_3 mass change and $m_{0Gd_2O_3}$ is the Gd_2O_3 initial mass. From stoichiometry of reaction 1, $\Delta m_{Gd_2O_3}$ is equal to $\Delta m/0.1510$, where Δm is the observed sample mass change. Therefore, the reaction degree is obtained from:

$$\alpha = \left(\frac{\Delta m}{0.151 \cdot m_{0Gd_2O_3}}\right) \quad (4)$$

Determination of kinetics parameters

In order to determine the kinetic parameters, it is first necessary to find the experimental conditions under which the reaction rate is not influenced by mass transfer processes (i.e., gaseous starvation, diffusion through the gaseous boundary layer, diffusion through the sample pores) [19].

The effect of the reagent gas velocity on the reaction rate was studied to determine the conditions where gaseous starvation and mass transfer limitations could be avoided. Figure 4 illustrates the effect of the flow rate on the chlorination of Gd_2O_3 at 723 K, chlorine pressure of 35 kPa and flow rates of 2, 4 and 8 L h^{-1}, which is the maximum flow rate that the experimental system can reach. Two curves of 4 L h^{-1} are presented to show the reproducibility of the system. It can be concluded that the supply rate of chlorine is not influencing the kinetics at this temperature.

Table 1 shows the values of chlorine diffusion rate through crucible top and experimental rate for $PCl_2 = 35$ kPa, Cl_2(g)–Ar(g) flow = 4 L h^{-1}, $m_o = 5$ mg and several temperatures. The rate values calculation was made using the Ranz and Marshall correlation [20], with the same procedure as described in the work "Kinetic Study of Europium Oxide Chlorination" [21]. The experimental rates at 723 K and lower temperatures are two or more orders of magnitude smaller than the calculated rates. These results are indicating that, at 723 K and temperatures below, the convective mass transfer through the boundary layer is not the rate-controlling step.

The effect of sample mass in the reaction rate was analyzed at 723 K, and it is shown in Fig. 5. It can be seen that the reaction rate measured as $d\alpha/dt$ does not depend on the sample mass at this temperature, and hence, an initial mass of 5 mg was used in the kinetic analysis.

The kinetic parameters of Gd_2O_3 chlorination were determined through isothermal TG between 623 and 723 K, with chlorine pressure of 35 kPa and initial mass of 5 mg. Figure 6 shows α-time curves. The activation energy (Ea) can be calculated by applying a "model-free" method [22, 23] from the slope of the plot ln time versus T^{-1}, where time is the time necessary to reach a given α value. The graphical representation of these results is shown in Fig. 7 for $\alpha = 0.2$, 0.4, 0.6 and 0.8. Average activation energy of 131 ± 2 kJ mol^{-1} was determined from linear regressions.

The experimental conversion versus time curves was analyzed with a conversion function that describes a reaction proceeding according to a nucleation and growth model (JMA model) [24–27]. This model is represented by the following equations:

Table 1 Comparison between calculated rate of diffusion through crucible top and experimental rate of reaction

Temperature/K	$10^6 \cdot N$ calculated/mol Cl_2 s^{-1} N_C	$10^9 \cdot N$ experimental/mol Cl_2 s^{-1} N_E	N_C/N_E
623	4.3	0.92	4675.9
673	4.6	5.7	804.5
698	4.7	15	318.6
723	4.8	28	171.4
773	5.1	89	57.3

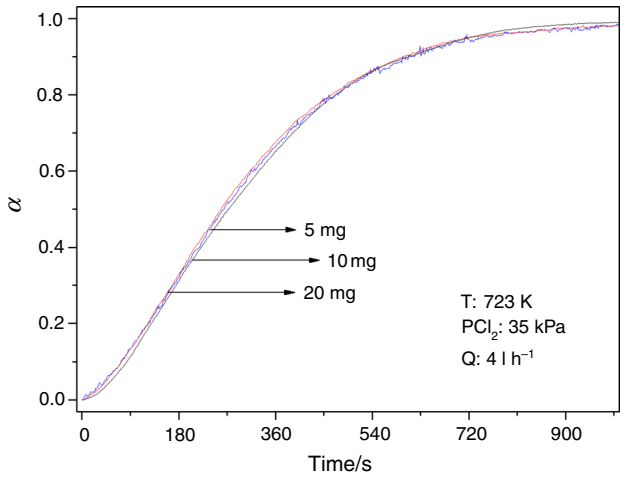

Fig. 5 Influence of sample mass in the chlorination of Gd_2O_3

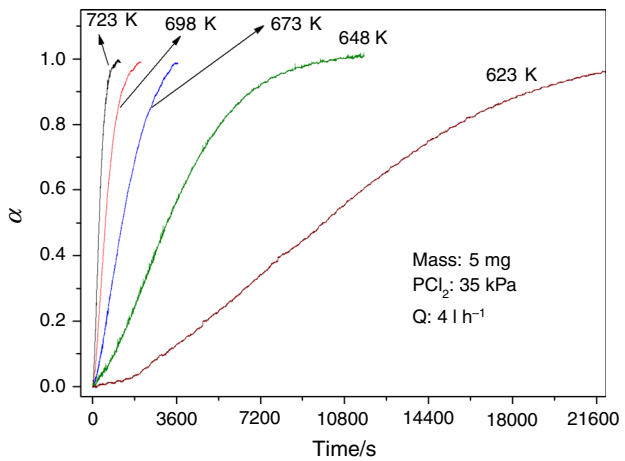

Fig. 6 Experimental conversion versus time curves for temperatures between 623 and 723 K

$$\alpha = 1 - \exp(-[k(T) \cdot t]^{n}) \quad (5)$$

$$k(T) = k_0 \cdot \exp\left(-\frac{Ea}{R_g \cdot T}\right) \quad (6)$$

where $k(T)$ is the global rate constant, k_0 is the pre-exponential factor, Ea is the effective activation energy, and n is

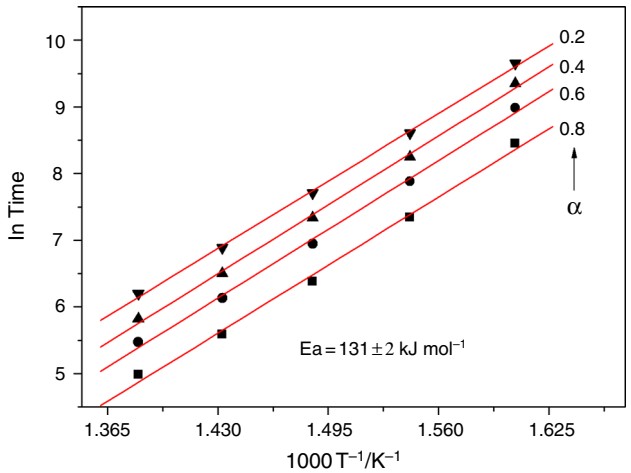

Fig. 7 ln time versus T^{-1} plots for the calculation of activation energy (Ea) by "model-free" method

the JMA exponent. The parameters k_0, Ea and n depend on the nucleation and growth mechanisms.

The conversion curves at $T \leq 723$ K were fitted with Eq. 5, and Table 2 shows the values of n, k and R (correlation coefficient) obtained from a nonlinear least squares fitting. Figure 8 shows the experimental curves (line graphs) and the fitted curves (scatter graphs), showing the good fit between them.

The nucleation models taken into account in the JMA description are continuous nucleation and site saturation. Kempen et al. [28] demonstrated numerically that intermediate values of the JMA exponents are possible for the combination of the different nucleation models and volume

Table 2 Values of parameters n and $k(T)$ obtained from the fits of conversion curves with the Johnson–Mehl–Avrami (JMA) model

T/K	10^4 $k(T)$/seg^{-1}	N	Correlation coefficient R
623	0.827	1.73	0.9992
648	2.47	1.58	0.9997
673	6.13	1.49	0.9998
698	14	1.52	0.9997
723	27.7	1.61	0.9996

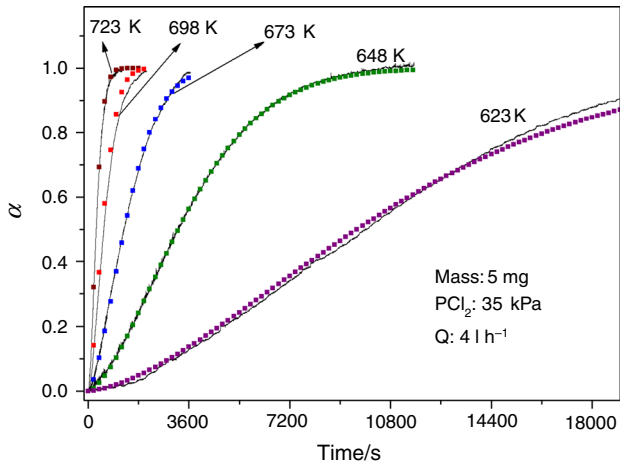

Fig. 8 Fits of the conversion curves with JMA equation. *Line graphs* experimental curves; *scatter graphs* calculated curves

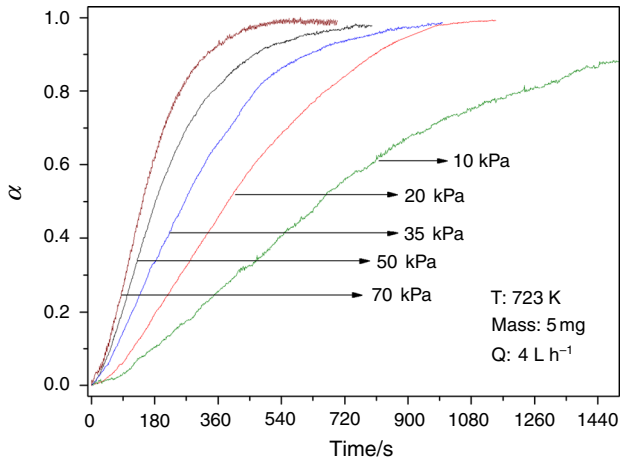

Fig. 10 Influence of pressure of $Cl_2(g)$ in the chlorination of Gd_2O_3

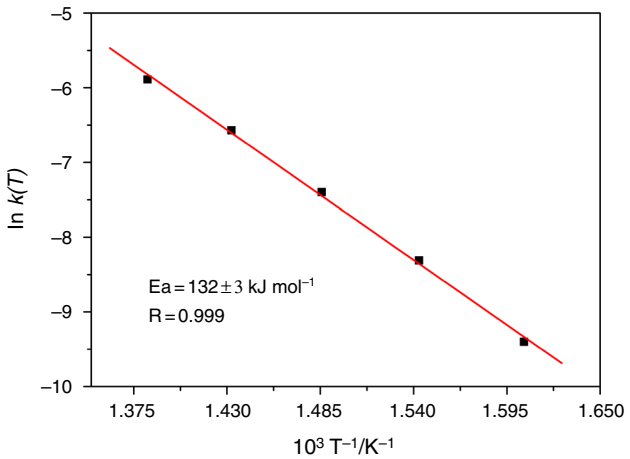

Fig. 9 ln $k(T)$ versus T^{-1} plot for the calculation of activation energy (Ea)

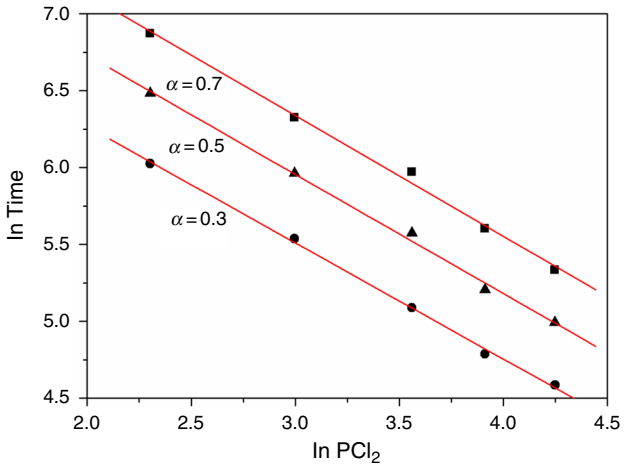

Fig. 11 ln time versus ln PCl_2 *plots* for the determination of the reaction rate order with respect to PCl_2

diffusion growth. The average value of n obtained was 1.59 ± 0.09. This value for the JMA exponent could be consistent with a three-dimensional growth and site saturation.

The activation energy in the temperature range of 623–723 K was calculated from the values of the global rate constant $k(T)$ through Eq. 6. Figure 9 shows the plot of ln k versus T^{-1}, from which a value for the activation energy of 132 ± 3 kJ mol^{-1} was obtained. This value is similar to the activation energy calculated by the "model-free" method (131 kJ mol^{-1}).

The general equation of heterogeneous solid–gas reaction rate is (assuming separable variables):

$$\frac{d\alpha}{dt} = K(T) \cdot F(PCl_2) \cdot G(\alpha) \quad (7)$$

The influence of PCl_2 was analyzed through experiments with different partial pressures of Cl_2 between 10 and 70 kPa at 723 K. Figure 10 shows these conversion versus time curves. To determine the reaction order with respect to PCl_2, Eq. 7 is integrated over time, $F(PCl_2)$ is assumed to have a form of $B \cdot PCl_2^x$ (where B is a constant, x is the reaction order with respect to PCl_2, and temperature is constant), and natural logarithms are applied. The resulting expression is:

$$-\ln t(\alpha) = H(\alpha) + x \cdot \ln PCl_2 \quad (8)$$

where $t(\alpha)$ is the time at which a conversion degree α is obtained at a temperature T and $H(\alpha)$ is a function that depends on α (since T is kept constant). From the slope of the straight lines of the $-\ln t(\alpha)$ versus ln PCl_2 plot for different conversion degrees, the reaction order x is obtained. The results are shown in Fig. 11. At 723 K, it was found that the reaction order with respect to partial pressures of Cl_2 is 0.77.

Global rate equation

The effects of parameters studied in Gd_2O_3(s) chlorination with the formation of GdOCl(s) could be expressed by a global rate expression according to Eq. 7 as follows:

$$\text{Rate}\left[s^{-1}\right] = \frac{d\alpha}{dt} = 6.6 \times 10^5 \left[s\,kPa^{0.77}\right]^{-1} \cdot e^{-(132\,kJ\,mol^{-1})/RT} \cdot (PCl_2[kPa])^{0.77} \cdot 1.59 \cdot (1-\alpha) \cdot [-\ln(1-\alpha)]^{0.37} \quad (9)$$

Isothermal reactions at temperature above 1123 K

Figure 12 shows the chlorination experiments at temperatures above 1123 K. It can be seen that after the formation of GdOCl, the reaction progresses with mass loss and the XRD analyses of the solid residues showed that GdOCl was the only phase present. The flow of Cl_2(g) was cut at 10,800 s in the chlorination performed at 1223 K. It was observed that the mass remains constant after this. By other side, the solid GdOCl was treated at 1223 K in argon atmosphere during 8 h and either mass or chemistry changes were not observed. Taking into consideration the preceding observations [21, 29, 30], the thermodynamic evaluation and the results obtained in the present investigation, the mass loss was caused by the chlorination of GdOCl(s) through reaction 3. The gadolinium trichloride formed at 1223 K is liquid, and its vapor pressures are 5.6×10^{-4} atm at 1223 K, sufficient vapor pressure to observe mass loss in the experimental system used. The reaction is carried out under a continuous flow which removes the vapor in equilibrium with the liquid.

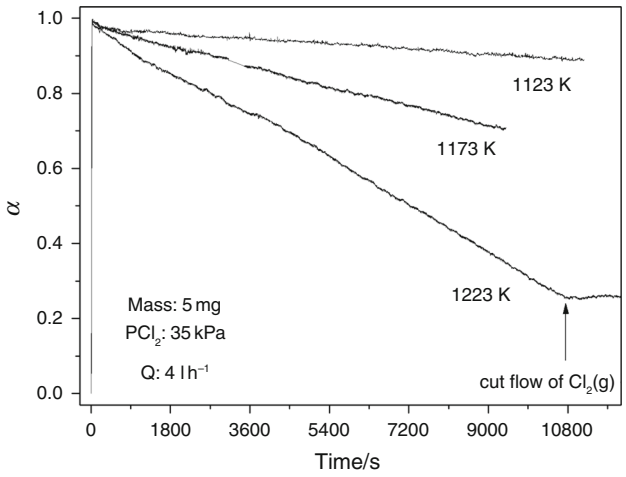

Fig. 12 Experimental conversion versus time curves for temperatures between 1123 and 1223 K

Characterization of gadolinium oxychloride

X-ray powder diffraction: Rietveld refinement

Powder XRD patterns were recorded using a Bruker D8-Advance X-ray powder diffractometer (Cu Kα radiation), with Bragg–Brentano geometry. In this case, the structure was refined by Rietveld refinement of the powder XRD data using the DIFFRAC^{plus} TOPAS 4.2 program [31]. For refinement, XRD data were collected in the 2θ ranges 10–120° with a step size of 0.02° using a 3 s/step scan speed.

X-ray powder diffraction data (Fig. 13) indicated that the product of the Gd_2O_3 chlorination at 1023 K is composed by a single phase of GdOCl, which crystallized in the tetragonal system possessing the Matlockite-type (PbFCl) structure (space group: P4/nmm). The detailed results of the Rietveld refinements are given in Table 3. The

Table 3 Rietveld refinement results for the X-ray powder pattern of the gadolinium oxychloride

Atom	*X*	*Y*	*Z*	Occupancy
Gd	0.0	0.5	0.17175	1
O	0.0	0.0	0.0	1
Cl	0.0	0.5	0.62734	1

Space group P4/nmm, $a = 3.9501376$ Å, $c = 6.6664518$ Å, $V = 104.02056$ Å^3

Rexp: 1.14, Rwp: 1.97, Rp: 1.37, R-Bragg = 2.289, GOF: 1.73

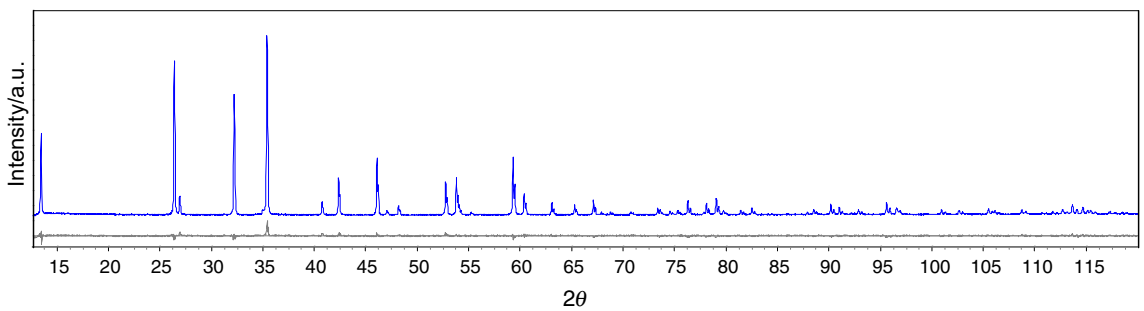

Fig. 13 Rietveld refinement of gadolinium oxychloride. Observed (*top*) and difference (*bottom*) profiles are shown

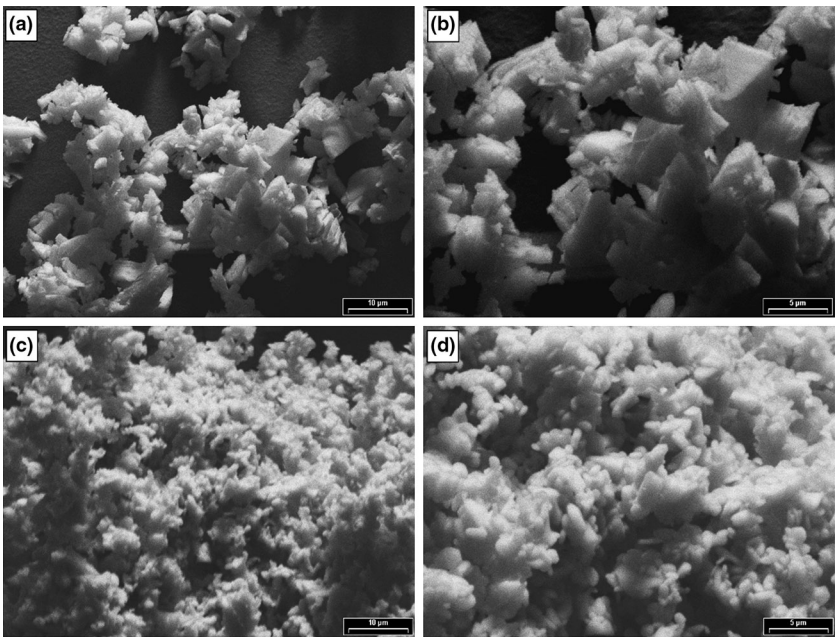

Fig. 14 SEM images of GdOCl produced at **a**, **b** 723 K and **c**, **d** 1223 K

goodness of fit of the GdOCl Rietveld final refinement is represented by GOF = R_{wp}/R_{exp}, and it has shown GOF = 1.73 as the best fit result.

Morphological analysis

Figure 14 shows the SEM images of the product at 723 K (a and b) and at 1223 K (c and d). The images show that the grain size of the GdOCl is different depending on the reaction temperature. At 1223 K, the grains are smaller than those obtained at 723 K.

Magnetic properties

The magnetic susceptibility measurements of GdOCl were taken with a Quantum Design SQUID magnetometer model MPMS2 between 2 and 300 K with an external magnetic field of 500 Oe. The experimental data were fitted with a function described by Curie–Weiss law: $\chi = C/(T-\theta)$, where χ is the magnetic susceptibility, C is the Curie constant, T is the absolute temperature, and θ is the Curie temperature measured in Kelvin.

Figure 15 shows the relation of molar magnetic susceptibility with the temperature, and the scatter graphs with open circles represent experimental points. Figure 16 shows the fit of the χ^{-1} versus T curve with Curie–Weiss law, and the parameters obtained were as follows: $\theta = -12.0 \pm 0.1$ K (which is similar to Gd_2O_3), $C = 7.9592 \pm 10^{-4}$ emu K mol^{-1}, estimated effective

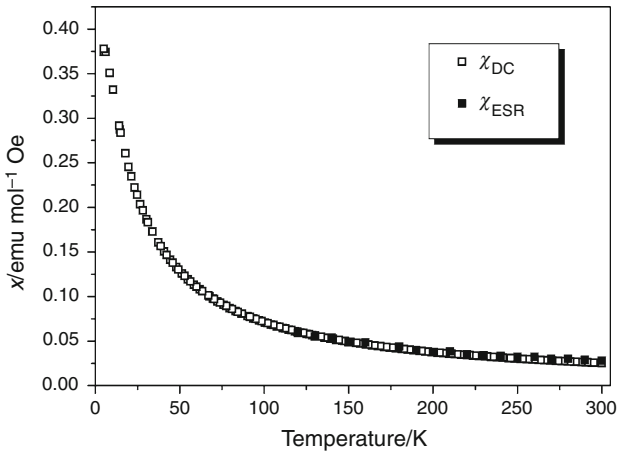

Fig. 15 χ versus T curves obtained by: *open square* magnetization measurement; *black square* ESR data

magnetic $\mu_{eff} = 7.98\mu_B$, which agrees with the theoretical and experimental values obtained for Gd^{+3} [32].

Figure 17 shows the electron spin resonance (ESR) data between 120 and 290 K measured every 10 K. ESR spectra were taken with a Bruker ESP300 spectrometer operating in X-band (9.5 GHz). The double integral of the ESR line is proportional to the constant-field (DC) susceptibility (χ_{ESR}). The integrals were normalized with a standard sample (Gd_2BaCuO_5 pattern), and the constant of proportionality was obtained. In Fig. 15 is observed the χ_{ESR} with black squares, and the data obtained overlap with the data of the magnetization (χ_{DC}).

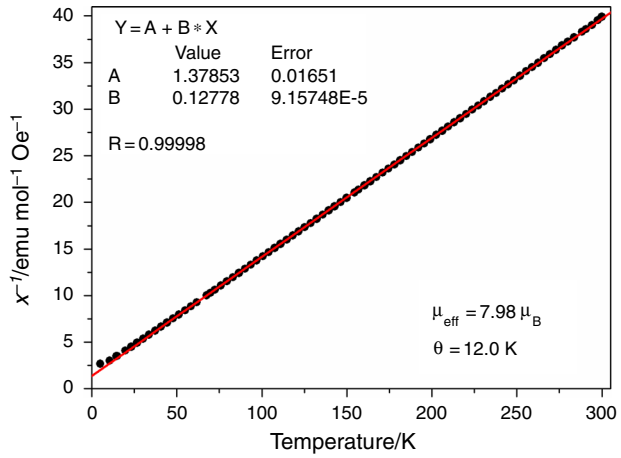

Fig. 16 Fits of the χ^{-1} versus T curves with Curie–Weiss law. *Scatter graphs* experimental curves; *line graphs* calculated curves

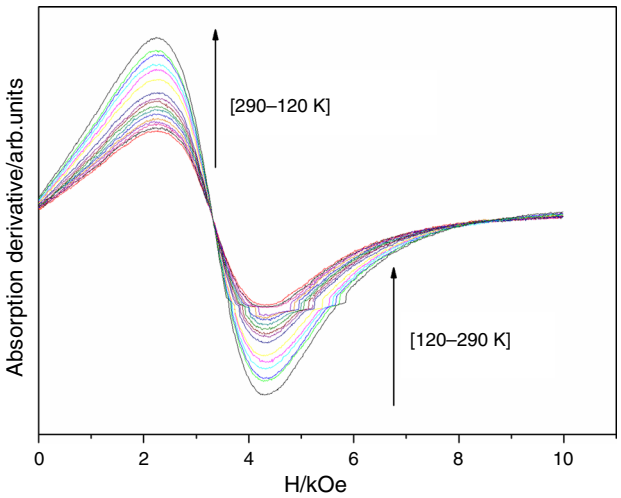

Fig. 17 ESR spectra of GdOCl for temperatures between 120 and 290 K

Conclusions

The kinetics and mechanism of the Gd_2O_3 chlorination with the formation of GdOCl have been established by TG analyses between 623 and 723 K and chlorine partial pressures ranging from 10 to 70 kPa.

The onset temperature of chlorination reaction was determined by non-isothermal TG at 600 K. Kinetic analysis showed that the reaction is under chemical control at 723 K. The formation of GdOCl proceeds through a nucleation and growth mechanism, and the conversion curves were analyzed with the Johnson–Mehl–Avrami description. The JMA parameters obtained were as follows: $Ea = 132$ kJ mol^{-1} and $n = 1.59$; the global rate equation can be obtained.

TGs isothermal at temperatures above 1123 K showed that GdOCl is further chlorinated to gadolinium trichloride.

The Rietveld refinements indicated that the GdOCl product crystallized in a tetragonal form of ROX possessing the Matlockite-type (PbFCl) structure, being P4/nmm the space group. The magnetic measurements indicated that the sample is paramagnetic at all the measurement ranges. The parameters obtained of Curie–Weiss law were as follows: $\theta = -12.0$ K, $C = 7.9592$ emu K mol^{-1} and estimated effective magnetic $\mu_{\text{eff}} = 7.98\mu_{\text{B}}$.

Acknowledgements The authors thank the Consejo Nacional de Investigaciones Científicas y Técnicas (CONICET), Universidad Nacional de Comahue and Agencia Nacional de Promoción Científica y Tecnológica (ANPCyT) for the financial support of this work and the Laboratorio de Resonancias Magnéticas of Centro Atómico Bariloche for the magnetic measurements and the information provided.

References

1. Binnemans K, Jones PT, Blanpain B, Gerven TV, Yang Y, Walton A, Buchert MJ. Recycling of rare earths: a critical review. Clean Prod. 2013;51:1–22.
2. Podkolzin SG, Stangland EE, Jones ME, Peringer E, Lercher JA. Methyl chloride production from methane over lanthanum-based catalysts. J Am Chem Soc. 2007;129(9):124569–76.
3. Mao JG. Structures and luminescent properties of lanthanide phosphonates. Coord Chem Rev. 2007;251:1493–520.
4. Zalas M. Gadolinium-modified titanium oxide materials for photoenergy applications: a review. J Rare Earths. 2014;32(6):487–95.
5. Gupta CK, Krishna Murthy N. Extractive metallurgy of rare earths. London: CRC Press; 2004.
6. Viyayan S, Melnyk AJ, Singh RD, Nuttall K. Rare earths: their mining, processing and growing industrial usage. Min Eng. 1989;41(1):13.
7. Korshunov BG, Georgievich B. Applications and potential uses of chlorination methods in metallurgy of non-common metals. Metall Rev Min Metall Inst Jpn. 1992;8:1–34.
8. Kanari N, Allain E, Joussemet R, Mochón J, Ruiz-Bustinza I, Gaballah I. An overview study of chlorination reactions applied to the primary extraction and recycling of metals and to the synthesis of new reagents. Thermochim Acta. 2009;495:42–50.
9. Mochizuki Y, Tsubouchi N, Sugawara K. Selective recovery of rare earth elements from Dy containing NdFeB magnets by chlorination. ACS Sustain Chem Eng. 2013;1(6):655–62.
10. Zhu G, Chi R, Shi W, Xu Z. Chlorination kinetics of fluorine-fixed rare earth concentrate. Min Eng. 2003;16(7):671–4.
11. Zhang X, He C, Wang L, Li Z, Feng Q. Synthesis, characterization and nonisothermal decomposition kinetics of $La_2(CO_3)\cdot 3.4H_2O$. J Therm Anal Calorim. 2015;119(3):1713–22.
12. Logvinenko V, Bakovets V, Trushnikova L. Dehydroxylation kinetics of gadolinium hydroxide. J Therm Anal Calorim. 2014;115(1):517–21.
13. Grivel JC. Thermal decomposition of $RE(C_2H_5CO_2)_3\cdot H_2O$ (RE = Dy, Tb, Gd, Eu and Sm). J Therm Anal Calorim. 2014;115(2):1253–64.
14. Yang HC, Cho YH, Eun HC, Kim EH. Kinetic analysis of a thermal dechlorination and oxidation of gadolinium oxychloride. J Therm Anal Calorim. 2007;90(2):379–84.
15. Pomiro FJ, Fouga GG, Gaviría JP, Bohé AE. Study of the reaction stages and kinetics of the europium oxide carbochlorination. Metall Mater Trans B. 2015;46B:304–15.

16. Rambabu U, Balaji T, Annapurna K, Buddhudu S. Fluorescence spectra of Tm^{3+}-doped rare earth oxychloride powder phosphors. Mater Sci Comput. 1996;43:195–8.
17. Rambabu U, Rajamohan Reddy K, Annapurna K, Balaji T, Satyanarayana J, Buddhudu S. Fluorescence spectra of Sm^{3+}-doped lanthanide oxychloride powder phosphors. Mater Lett. 1996;27(1-2):59–63.
18. HSC 6.12. Chemistry for windows. Finland: Outokumpu Research Oy, Pori; 2007.
19. Kim SK. The determination of the kinetics of gas–solid reactions by the nonisothermal technique. Ph.D. Thesis, University of Utah; 1981.
20. Ranz WE, Marshall WR. Evaporation from drops. Parts I and II. Chem Eng Prog. 1952;48(141–6):173–80.
21. Pomiro FJ, Fouga GG, Bohé AE. Kinetic study of europium oxide chlorination. Metall Mat Trans B. 2013;44B:1509–19.
22. Vyazovkin S. Model-free kinetics. J Therm Anal Calorim. 2006;83:45–51.
23. Mamleev V, Bourbigot S, Le Bras M, Lefebvre J. Three model-free methods for calculation of activation energy in TG. J Therm Anal Calorim. 2004;78:1009–27.
24. Avrami M. Kinetics of phase change. I: general theory. J Chem Phys. 1939;7(12):1103–13.
25. Avrami M. Kinetics of phase change. II Transformation-time relations for random distribution of nuclei. J Chem Phys. 1940;8(2):212–24.
26. Avrami M. Granulation, phase change, and microstructure kinetics of phase change. III. J Chem Phys. 1941;9(2):177–84.
27. Johnson WA, Mehl RF. Reaction kinetics in processes of nucleation and growth. Trans Am Inst Min Metall Eng. 1939;135:416–27.
28. Kempen ATW, Sommer F, Mittemeijer EJ. Determination and interpretation of isothermal and non-isothermal transformation kinetics; the effective activation energies in terms of nucleation and growth. J Mater Sci. 2002;37(2):1321–32.
29. Gaviría JP, Navarro LG, Bohé AE. Chlorination of lanthanum oxide. J Phys Chem A. 2012;116:2062–70.
30. Bosco MV, Fouga GG, Bohé AE. Kinetic study of neodymium oxide chlorination with gaseous chlorine. Thermochim Acta. 2012;540:98–106.
31. TOPAS. Version 4.2. Germany: Bruker AXS, Karlsruhe; 2008.
32. Moon RM, Koehler WC. Magnetic properties of Gd_2O_3. Phys Rev B. 1975;11(4):1609–22.